Sum Frequency Generation Study of Langmuir Blodgett Film Architecture

T. P. Johansson and G. W. Leach*

Department of Chemistry, Simon Fraser University, 8888 University Drive, Burnaby, British Columbia V5A 1S6, Canada

Received: February 7, 2006; In Final Form: May 12, 2006

We present sum frequency generation vibrational spectroscopy data on monolayer films of pure stearonitrile and mixed films of stearonitrile and ferric stearate deposited by the Langmuir Blodgett technique. Films ranging in composition from pure stearonitrile to 65% stearonitrile/35% ferric stearate deposit in a head-to-tail, Z-type architecture while films of composition <65% stearonitrile deposit in a head-to-head, tail-to-tail, Y-type structure. The vibrational spectra of the monolayer films corresponding to these two different architectures show distinct and characteristic features in their CH stretching regions. Spectral analysis indicates little difference in the modes associated with the terminal methyl groups but large differences in the methylene CH_2 vibrational modes. These spectral differences are consistent with alkyl chains that possess uncompensated methylene oscillator strength arising from portions of the chain that are bent. This behavior is consistent with the energetics expected from a close-packed monolayer of stearonitrile molecules whose CN headgroups possess sizable dipole moments and are expected to adopt a large center-to-center angle to minimize electrostatic, dipole−dipole repulsive interactions.

Introduction

The Langmuir Blodgett (LB) technique is a commonly used method to deposit monolayers of amphiphilic materials onto solid substrates to form thin solid films.[1−3] Interest in this deposition method derives from its ability to form well-ordered thin films with a variety of potential technological applications, depending upon the nature of the individual amphiphiles comprising the resultant thin film structures. Polar multilayer structures, for example, can show pyroelectric, piezoelectric, ferroelectric, and/or nonlinear optical effects. These macroscopic effects result from the coherent summation of responses of the amphiphiles in individual layers and thus rely on well-defined film architectures.

Langmuir Blodgett film architectures generally fall into three categories. The most common and most thermodynamically stable multilayer film structure is the so-called Y-type structure in which monolayers are deposited in a head-to-head and tail-to-tail configuration. These multilayer structures are generally nonpolar unless prepared in an ABAB... arrangement of alternating polar (A) and inert (B) amphiphiles. Y-type film structures arise when favorable interactions between the amphiphile's headgroups and between tails are dominant. This structure typifies long-chain fatty acid multilayers where dimerization of headgroups in adjacent layers and hydrophobic interactions of the terminal methyl groups in adjacent layers stabilize the nonpolar film structure. In contrast, less stable Z-type (X-type) films are comprised of amphiphiles that deposit in a head-to-tail arrangement on hydrophilic (hydrophobic) substrates and thus result in an overall polar multilayer structure. Y-type LB structures are characterized by deposition on both up and down strokes, as the substrate passes through the amphiphilic monolayer on the water surface. Z-type and X-type polar structures are obtained only when deposition occurs on one of the passes—the up stroke for Z-type and down stroke for X-type structures.

Controlling the architecture of LB films and constructing polar Z-type multilayer structures has remained a significant challenge. While several examples of Z-type deposition have been reported,[4−8] it has remained difficult to design and predict film architecture on the basis of the chemical functionality of the building blocks within the amphiphile. These difficulties are compounded by the observation that in some cases, even for amphiphiles that are deposited in polar multilayer structures, subsequent structural rearrangement of the films to the more stable Y-type structure can occur. It is generally accepted that deposition behavior is dictated by the surface wettability of the previously deposited layer.[4] To favor the deposition of polar Z-type multilayers, one needs to discourage deposition on the down stroke and encourage deposition on substrate withdrawal. This requires significant hydrophilicity of the surface after each stroke (both advancing and receding aqueous contact angles <90°), while maintaining overall amphiphilic character. Strategies for the design of Z-type architectures that have met with some success have thus focused on controlling the number and position of polar groups within the otherwise hydrophobic long chains of the amphiphiles.[4] Nevertheless, little is known on a molecular level about the detailed orientations and interactions within the monolayer films that are responsible for film architecture.

Here, we present studies of the simple amphiphile stearonitrile ($CH_3(CH_2)_{16}CN$) in pure and mixed monolayer and multilayer films. We have investigated the film structure and average chain orientations in films of pure and mixed films of stearonitrile and ferric stearate ($Fe(CH_3(CH_2)_{16}COO)_3$). We have shown that by controlling the film composition we can control the multilayer architecture through the fabrication of either Z- or Y-type structures. Sum frequency generation (SFG) vibrational spectroscopy of the monolayer films indicates characteristic differ-

* Author to whom correspondence should be addressed. Phone: (604) 291-5493. Fax: (604) 291-3765. E-mail: gleach@sfu.ca.

10.1021/jp060804m CCC: $33.50
Published on Web 07/28/2006

ences in the chain morphologies between the films that define these different deposition modes.

Experimental Section

Monolayer and multilayer films of stearonitrile, ferric stearate, and their mixtures were prepared using standard Langmuir Blodgett protocols. Specifically, amphiphiles were spread from chloroform solutions (~1.00 mg/mL) onto a pure water subphase (18.2 MΩ cm) contained within a polytetrafluoroethylene (PTFE) LB trough (Nima 600). Surface pressures were measured using a Wilhelmy plate balance. After chloroform evaporation, the films were compressed at a rate of 10 cm^2/min to record surface pressure/area isotherms. Langmuir Blodgett monolayer and multilayer films were obtained by compression to a surface pressure of 20 mN/m and equilibration for 10 min and were followed by deposition onto hydrophilic substrates at a dipping rate of 15 mm/min. Multilayer films were fabricated by deposition onto clean microscope slides prepared by immersion in an acid/piranha bath for 10 min followed by extensive washing with water. Monolayer films for SFG study were prepared on the hypotenuse of a CaF_2 right-angle prism held in a mount designed in-house for this purpose. For these studies, the substrate was held in the water subphase until the monolayer was prepared and deposition occurred upon substrate withdrawal through the water surface.

Film structure and quality were inferred by deposition ratio measurement, X-ray diffraction studies, and atomic force microscopy (AFM). Low-angle X-ray diffraction experiments were carried out using a RAPID (Rigaku) X-ray diffractometer with a copper target ($\lambda_{K\alpha}$ = 1.542 Å) and an image plate detector. X-ray diffraction patterns were obtained using a 500 μm collimator inserted into the path of the incident X-rays. Atomic force microscopy studies were carried out using a TM Microscopes Explorer scanning probe microscope system. Atomic force microscopy measurements were taken to assess the overall quality of the films and to determine film thickness. Film thickness measurements were obtained by scratching a portion of the film from the substrate and measuring the height of the unperturbed film in comparison to the region where the film had been removed.

Sum frequency generation spectra in the CH region were obtained using the tunable, broadband, 100 fs mid-IR light produced by difference frequency generation of the signal and idler beams from a home-built optical parametric amplifier (OPA). The OPA was pumped by the output of a regenerative amplifier (Positive Light) operating at a nominal wavelength of 800 nm and possessing typical pulse energies of 1 mJ and a 1 kHz repetition rate. Upconversion of the IR polarization is achieved with residual 800 nm light unused in the parametric amplifier, following spectral and temporal manipulation. We have previously used this apparatus to monitor the spectroscopy and coherent vibrational dynamics in an amphiphilic monolayer.[9] The apparatus is capable of variable resolution spectral domain studies with a resolution determined by the bandwidth of the 800 nm light. For the studies presented here, the spectral resolution was typically 8 cm^{-1}. The broadband SFG signals generated from the surface are dispersed in a spectrograph (Oriel 260i) and collected with an electron-multiplying charge coupled device (CCD) camera (Andor). Sum frequency generation spectra have been collected in four polarization combinations. Polarization control in the infrared is achieved with a multi-wavelength CaF_2 wave plate (Alphalas), polarization control at 800 nm is accomplished with a zero-order half wave plate (CVI), and the SFG signal is polarization selected with a quartz Glan-Thompson polarizer (CVI). In our analysis, all spectra have been normalized for infrared intensity differences to the nonresonant SFG signal from a thin film of malachite green.

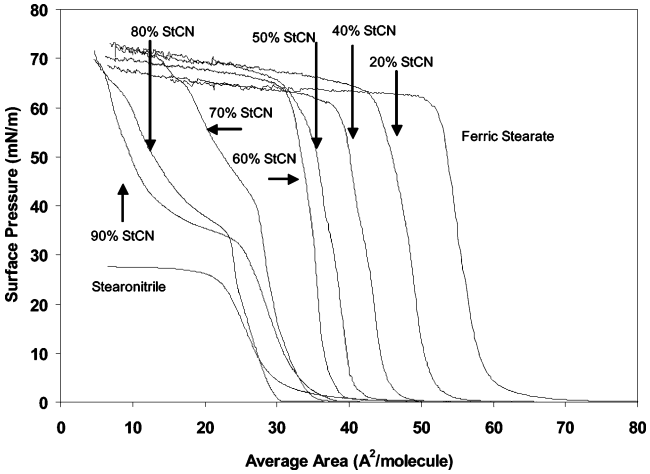

Figure 1. Pressure−area isotherms of mixed films of stearonitrile and ferric stearate of various compositions. Isotherms of increasing stearonitrile mole fraction are displayed from right to left.

While our SFG experiments were performed on monolayer films deposited onto CaF_2 substrates and the transfer ratio, X-ray diffraction, and AFM measurements were performed on multilayer structures deposited onto glass substrates, we have confirmed by transfer ratio measurements that both substrates yield similar multilayer film architectures despite having different surface characteristics.

Results and Discussion

Figure 1 shows the surface pressure/area ($\pi-A$) isotherms for pure stearonitrile (SN),[10] pure ferric stearate (FS),[11] and selected mixed films of the two. Upon compression, the isotherm of pure SN shows a slow increase in surface pressure beginning at a molecular area of approximately 45 $Å^2$/molecule. At a molecular area of approximately 30 $Å^2$/molecule the rate of increase of surface pressure with barrier compression increases smoothly until a surface pressure of ~25 mN/m is reached. Further compression leads to film collapse. The shape and low slope of the $\pi-A$ curve for the pure SN monolayer indicate that SN forms a weakly stable liquid condensed (LC) monolayer. The isotherm of ferric stearate is characterized by a much sharper rise in surface pressure. The onset of pressure increase begins at an area of 75 $Å^2$/molecule and continues until a collapse pressure of 63 mN/m is reached at an area of 50 $Å^2$/molecule, consistent with the behavior of a solid condensed phase. Isotherms of the mixed films show intermediate behavior. In particular, the isotherms of mixed films of composition 10−60% stearonitrile resemble the isotherm of pure ferric stearate in shape and curvature but are systematically displaced to smaller areas, as expected by the smaller area per molecule of stearonitrile. In contrast, the isotherm corresponding to 70% SN shows a significantly different behavior to those of lower SN composition. The initial increase in surface pressure resembles that of isotherms of lower SN composition; however, at a surface pressure of ~40 mN/m the isotherm displays a distinct reduction in slope and a smooth increase in surface pressure thereafter. This feature appears to be common to all isotherms with a composition of 70% SN or greater and appears to define the onset of a new phase. Interestingly, the position of this onset in isotherms of larger SN composition is displaced to smaller

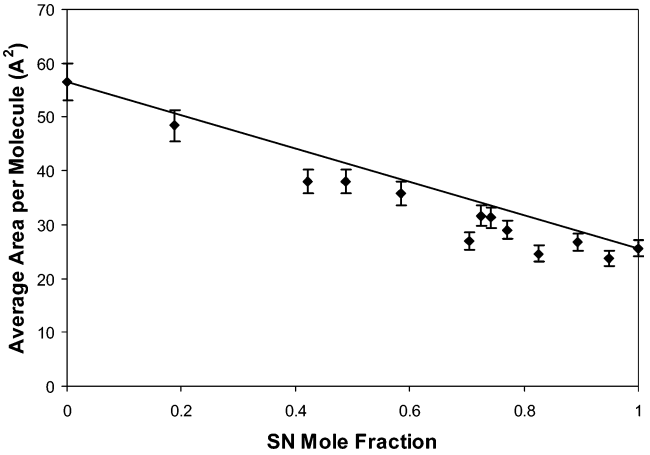

Figure 2. Plots of average area vs mole fraction of stearonitrile. The area is taken as the area at 20 mN/m. The solid line represents the expected trend in area per molecule of two immiscible components as described by eq 1.

surface pressures, and this new region of the isotherm shows an increase in curvature with increasing SN composition.

Information regarding the extent of mixing in the two-component films can be extracted from the isotherms in Figure 1. For a mixture of immiscible components, the film can be thought of as being composed of separate monolayers. The area occupied by the film will be the sum of the areas of the separate films. For a two-component mixture

$$A = \chi_1 A_1 + \chi_2 A_2 \tag{1}$$

where the χ_i are the mole fractions of the individual film components, and A_i their corresponding molecular areas in the single-component films at the same surface pressure. Thus a plot of A versus χ_1 should be a straight line. Deviation from this relationship provides evidence for miscibility. Figure 2 shows such a plot for mixed films of stearonitrile and ferric stearate. The data show evidence of a negative deviation from this linear relationship, consistent with the notion that these materials are miscible.

The packing density of the monolayers can be evaluated and compared by the two-dimensional compressibility[12]

$$C_s = -\left(\frac{1}{A}\right)\left(\frac{\partial A}{\partial \pi}\right)_T \tag{2}$$

which can be extracted from the $\pi-A$ isotherms. The compressional modulus (C_s^{-1}) is often used to characterize the nature of a monolayer's stable phases and has been correlated with particular phase behavior.[12] Specifically, a maximum value of the compressional modulus in the range of 100−250 mN/m is characteristic of the liquid condensed phase while a value of C_s^{-1} between 600 and 2000 mN/m is characteristic of the solid condensed phase. Figure 3 shows a plot of the maximum C_s^{-1} values obtained by analysis of the isotherms according to eq 2. Note that for isotherms with more than one stable phase, multiple peaks of the compressional modulus can occur. In Figure 3, these have been associated with either the low-pressure or the high-pressure regimes. From Figure 3 it is apparent that with an increasing SN composition the maximum in the compressional modulus decreases and does so in a dramatic way in the composition range of ∼65% SN/35% FS. In this region, the value of C_s^{-1} drops from values characteristic of a solid condensed phase to those consistent with a liquid condensed phase. On the basis of these data and the appearance

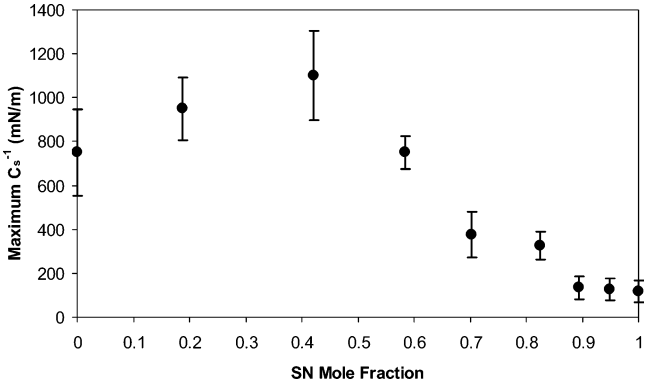

Figure 3. Maximum inverse compressibility plotted vs mole fraction of stearonitrile.

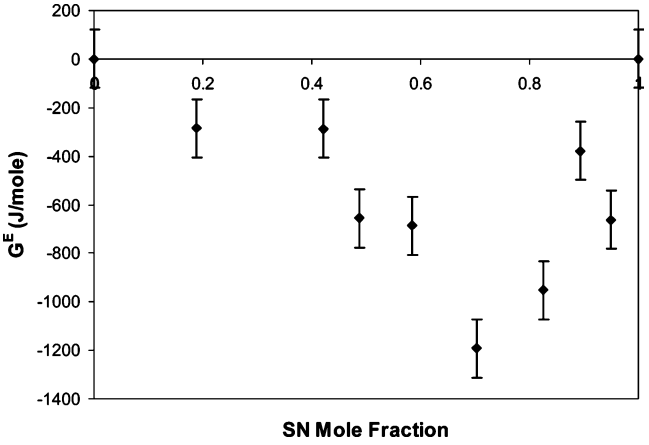

Figure 4. Plots of the calculated Gibbs excess energy vs mole fraction of stearonitrile taken as the integral of the area over a pressure range from 0 to 20 mN/m.

of the $\pi-A$ isotherms, we assign the onset of new features in the isotherms to the appearance of a LC phase at compositions of ∼65% SN and greater.

The isotherms also provide a means of determining the extent of component mixing within films. The Gibbs energy of mixing is given by

$$\Delta G_{\text{mix}} = \Delta G_{\text{ideal}} + G^E(\pi) \tag{3a}$$

where ΔG_{ideal} is the Gibbs energy of mixing of an ideal mixture

$$\Delta G_{\text{ideal}} = RT(\chi_1 \ln \chi_1 + \chi_2 \ln \chi_2) \tag{3b}$$

and the excess Gibbs energy, $G^E(\pi)$, is a measure of the desorption energy arising from cohesive forces within the monolayer.[12,13] The excess Gibbs energy can be evaluated from the experimental isotherms by

$$G^E(\pi) = \int_{\pi=0}^{\pi} [A - (\chi_1 A_1 + \chi_2 A_2)]\, d\pi \tag{3c}$$

The values of $G^E(\pi)$ for a surface pressure of 20 mN/m are shown in Figure 4. Since ΔG_{ideal} is always negative, $G^E(\pi)$ values that are negative indicate an overall ΔG_{mix} that is negative and support the idea of film miscibility. Figure 4 shows that the Gibbs excess is a minimum in the region where film deposition behavior changes.

Deposition of multilayer films onto hydrophilic substrates revealed that film architecture was dependent upon the film composition. Figure 5 shows the deposition ratios for multilayer films of pure stearonitrile as well as those for a mixed film of

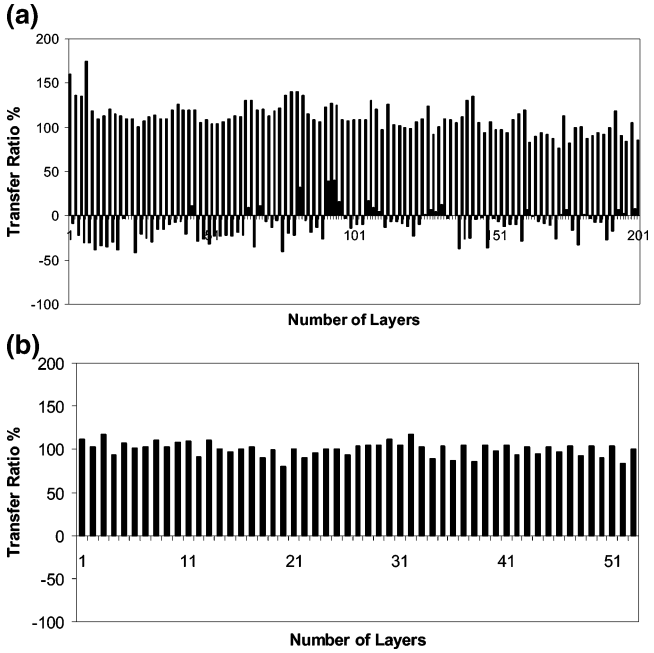

Figure 5. Histograms showing the apparent transfer ratios of a monolayer of (a) stearonitrile and (b) a mixed film of 40% stearonitrile and 60% ferric stearate on a hydrophilic glass slide. Odd numbers represent upstrokes. Even numbers represent downstrokes.

composition 40% SN/60% FS. The data indicate near unity transfer ratios on the upstroke and near zero transfer ratios on the downstroke for pure SN film deposition and near unity transfer ratios on both the upstroke and the downstroke for the mixed film deposition. These deposition ratios are signatures of Z- and Y-type multilayer film architectures, respectively. Multilayer films prepared for a range of film compositions indicated that deposition behavior fell into either one of these two categories. Specifically, deposition of multilayer films ranging in composition from pure SN to ~70% SN show deposition ratios consistent with Z-type architectures while deposition ratios for mixed films with a composition of ~60% or less SN show behavior consistent with Y-type film structure.

The proposed film architectures were corroborated by X-ray diffraction studies. Figures 6a and 6b show the X-ray diffraction patterns for a 30-layer film of pure FS and a 102-layer film of pure SN, respectively. The diffraction pattern of FS shows peaks of substantial diffraction intensity at 1.98°, 3.69°, 5.6°, 7.45°, and 9.39°, consistent with the incorporation of metal cation into the multilayer structure. These diffraction peaks are separated by roughly 1.85°, corresponding to a spacing of 4.76 nm. This distance is consistent with the bilayer spacing expected for a Y-type film consisting of a head-to-head, tail-to-tail architecture in which each alkyl chain is fully extended in an all-trans configuration. The X-ray diffraction pattern of SN displays three peaks at angles of 1.4°, 2.4°, and 4.0°, respectively. Unlike the case of FS, these peaks are not evenly spaced as one would expect for an ordered layered structure. To determine the nature of these peaks, this experiment was repeated by rocking the input angle of the X-rays to identify peaks that may arise from X-ray reflections from the film and substrate interfaces. Because of the weak diffraction intensity expected from a film composed almost entirely of carbon, even weak reflections of the X-ray beam can generate pronounced peak intensities that preclude correct X-ray diffraction assignment. Rocking of the sample is expected to wash out peaks due to reflection relative to those due to film diffraction. As can be seen by the bottom trace of Figure 6b, the two intense low-angle peaks appearing in the

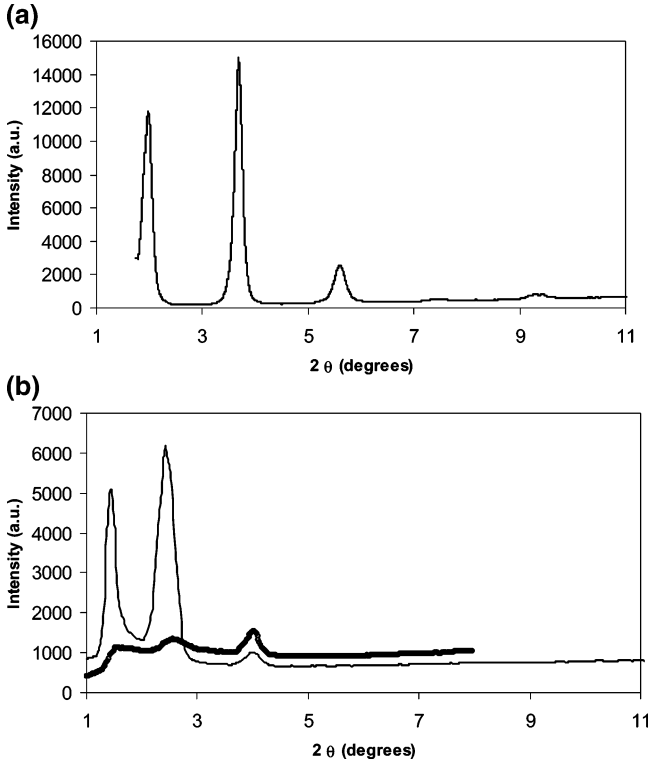

Figure 6. Low-angle X-ray diffraction pattern of (a) a 30-layer film of ferric stearate and (b) a 100-layer film of stearonitrile. Solid lines represent diffraction using a constant angle of incidence. Circles represent the diffraction pattern obtained by rocking the sample to vary the angle of incidence.

upper trace of Figure 6b are markedly reduced in intensity compared to the third peak, which now appears with the greatest diffraction intensity. On this basis, we attribute the peaks appearing at 1.4° and 2.4° to reflections and assign the peak at 4.0° to film diffraction. This diffraction peak corresponds to a *d* spacing of 22 Å, slightly smaller than that expected from a fully extended all-trans chain of SN (24 Å) but consistent with the proposed head-to-tail deposition architecture.

Film thickness measurements using AFM were conducted on both pure SN and mixed 40% SN/60% FS films. Film thickness measurements of a pure, 30-layer SN film yielded an overall thickness of 70.5 ± 8 nm, averaged over three measurements at different positions on the same film. This overall thickness corresponds to an average monolayer thickness of 2.35 nm, in good agreement with the *d* spacing obtained via X-ray and the thickness expected for deposition on every second stroke. Atomic force microscopy measurements on a 61-layer film with a composition of 40% SN/60% FS yielded an average thickness of 148.98 ± 22 nm, corresponding to an average monolayer thickness of 2.44 nm and consistent with deposition on both the upstroke and the downstroke during LB deposition.

Given the differences in film deposition behavior, we undertook an examination of the average orientation of the amphiphiles in the pure and mixed monolayers via sum frequency generation studies. Our goal was to establish whether one could find a correlation between the film deposition behavior and the amphiphile orientation.

Figure 7 shows the SFG spectra in the CH region obtained under three different polarization conditions for monolayer films of composition 80% SN/20% FS and 40% SN/60% FS. (Four polarization combinations were collected, but for the sake of clarity, only three are displayed since the SPS and PSS polarization combinations are very similar.) The vibrational

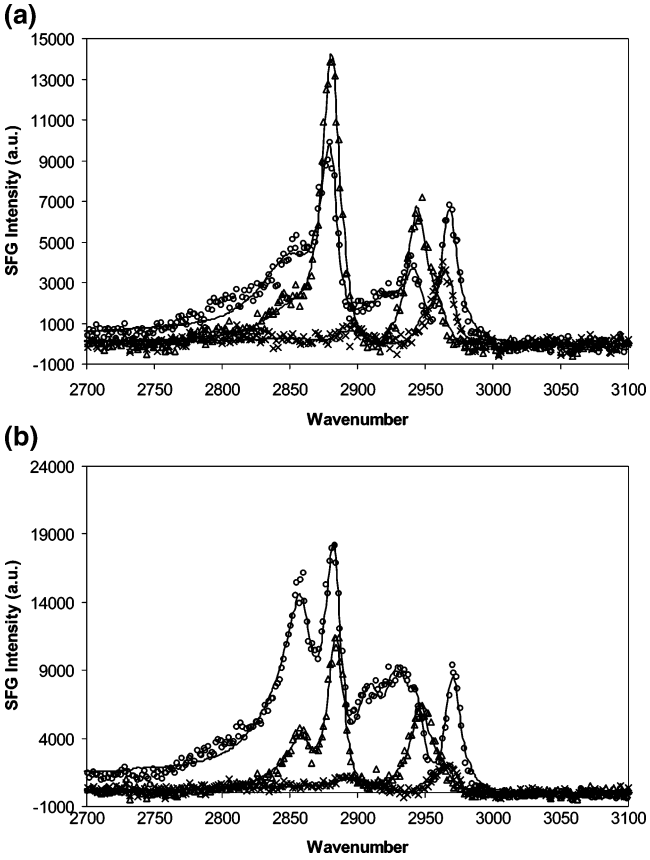

Figure 7. Circles, triangles, and X's represent the PPP, SSP, and SPS spectra, respectively, of (a) 40% stearonitrile/60% ferric stearate and (b) 80% stearonitrile/20% ferric stearate. Solid lines are the fitted curves.

mode assignments in this spectral region are well-known.[14,15] The vibrational modes at 2880, 2965, and 2940 cm^{-1} are attributed to the methyl group and have been assigned as the symmetric stretch (r+), the asymmetric stretch (r−), and Fermi resonance (FR) between the symmetric stretch and two quanta of the bending mode. The modes at 2850 and 2920 cm^{-1} have been assigned to the symmetric (d+) and asymmetric (d−) stretches of the CH_2 groups. The mode appearing at 2910 cm^{-1} has been assigned as a methylene symmetric stretch Fermi resonance.

Inspection of Figures 7a and 7b indicate substantial differences between the spectra obtained in the PPP and SSP polarization combinations for the films of different compositions (polarization combinations refer to the sum frequency signal, 800 nm, and infrared polarizations, respectively). It should be noted that the spectra displayed in Figure 7b are characteristic of all films with a composition of 70% SN or greater, while the spectra of Figure 7a are characteristic of all monolayer films with a composition of 60% SN or less. That is, there is a clear correlation between the characteristics of film composition, film deposition behavior, and the films' characteristic spectral signatures.

A thorough analysis of the spectra in Figure 7 has been undertaken. Here, we present a description of how one derives molecular orientation information from the SFG spectra.[16] Irradiation from two optical fields $\mathbf{E}_1$ and $\mathbf{E}_2$ with frequencies ω_1 and ω_2 generates a second-order nonlinear polarization

$$\mathbf{P}^{(2)}(\omega = \omega_1 + \omega_2) = \chi^{(2)}_{\text{eff}}:\mathbf{E}_1(\omega_1)\mathbf{E}_2(\omega_2) \tag{4}$$

where

$$\chi^{(2)}_{\text{eff}} = [\mathbf{e}(\omega)K(\omega)]\,\chi^{(2)}:[\mathbf{e}(\omega_1)L(\omega_1)]\,[\mathbf{e}(\omega_2)L(\omega_2)] \tag{5}$$

and **e** is the unit polarization vector, L is the linear Fresnel factor describing the incident electric fields at the interface, and K is a combination of linear and nonlinear Fresnel factors describing the outgoing SFG field.[17,18] L and K are both geometry-dependent and dependent on how one models the refractive index (n) of the film.[16] The macroscopic $\chi^{(2)}$ is related to the microscopic molecular hyperpolarizability by

$$\chi^{(2)}_{ijk} = N\,\Sigma\langle R_{ii'}R_{jj'}R_{kk'}\rangle\alpha_{i'j'k'} \tag{6}$$

where α is the molecular hyperpolarizability tensor, the broken brackets represent the average over the adsorbate orientation obtained from the Euler rotation tranformation matrix from the molecular frame (*ijk*) to the lab frame (*IJK*), and N is the number of surface-active species. If α is known, then by measuring $\chi^{(2)}_{IJK}$, one can deduce the average orientation of the vibrational mode in question.

If the IR frequency is near a vibrational resonance, then α and χ can be described by Lorentzian line shape functions

$$\alpha = \alpha_{\text{nr}} + \Sigma\,\Lambda/(\omega - \omega_0 - i\Gamma) \tag{7}$$

$$\chi = \chi_{\text{nr}} + \Sigma\,A/(\omega - \omega_0 - i\Gamma) \tag{8}$$

where ω_0 is the resonant frequency of the vibrational mode, Γ its associated Lorentzian half-width, ω the frequency of the infrared radiation, Λ the molecular hyperpolarizability of the individual vibrational modes, α_{nr} the nonresonant hyperpolarizability, A the macroscopic strength factors for individual vibrational modes, and χ_{nr} the nonresonant susceptibility.

The orientation of the terminal CH_3 group can be determined by analyzing its symmetric stretch mode as well as its asymmetric stretch mode. The CH_3 group possesses C_{3v} symmetry and has three nonzero independent elements in its hyperpolarizability tensor, α_{zzz}, $\alpha_{xxz} = \alpha_{yyz}$ (associated with the r+ mode), and α_{zxx} (associated with the r− mode). Assuming an isotropic sample and averaging over Euler angles yields[17,19]

$$\chi_{yyz} = \chi_{xxz} = {}^1/_2 N\alpha_{zzz}[\langle\cos\theta\rangle(1 + R) - \langle\cos^3\theta\rangle(1 - R)] \tag{9a}$$

$$\chi_{zzz} = N\alpha_{zzz}[\langle\cos\theta\rangle(R) + \langle\cos^3\theta\rangle(1 - R)] \tag{9b}$$

$$\chi_{yzy} = \chi_{zyy} = \chi_{xzx} = \chi_{zxx} = {}^1/_2 N\alpha_{zzz}[\langle\cos\theta\rangle - \langle\cos^3\theta\rangle(1 - R)] \tag{9c}$$

where $R = \alpha_{xxz}/\alpha_{zzz}$. Similar expressions hold for the CH_3 asymmetric stretch mode

$$\chi_{yyz} = \chi_{xxz} = -{}^1/_2 N\alpha_{zxx}[\langle\cos\theta\rangle - \langle\cos^3\theta\rangle] \tag{10a}$$

$$\chi_{zzz} = -2\chi_{yyz} = N\alpha_{zxx}[\langle\cos\theta\rangle - \langle\cos^3\theta\rangle] \tag{10b}$$

$$\chi_{yzy} = \chi_{zyy} = \chi_{xzx} = \chi_{zxx} = {}^1/_2 N\alpha_{zxx}[\langle\cos^3\theta\rangle] \tag{10c}$$

The presence of the Fermi resonance band perturbs the intensity of the r+ mode. To evaluate the unperturbed intensity, the following expression has been used

$$A_{\text{unperturbed}}(\text{r+}) = (A(\text{r+})^2 + A(\text{FR})^2)^{1/2} \tag{11}$$

TABLE 1: Parameters Resulting from the Simultaneous Fitting of the SSP, PPP, SPS, and PSS SFG Spectra of the Mixed Film with a Composition of 80% Stearonitrile/20% Ferric Stearate

A_{SSP}	A_{PPP}	A_{SPS}	A_{PSS}	ω_0 (cm^{-1})
760.2	670.7	−25.7	−73.4	2884
564.5	375.8	−98.2	−193.7	2944
−168.1	829.0	525.1	435.1	2970
572.5	794.8	23.1	−48.4	2861
149.8	531.3	207.9	−38.9	2910
381.7	814.9	136.6	92.3	2931

	χ_{nr}	phase		Γ (cm^{-1})
SSP	8.7	90.4	CH_3	7.4
PPP	29.7	190.0	CH_2	11.7
SPS	17.1	146.1		
PSS	3.6	−134.0		

TABLE 2: Orientation Angles (deg) of the Methyl Group Calculated Using Various Methods as Discussed in the Text

SN mole fraction	I	II	III	IV	average of I, II, and III	standard deviation
0	43.7/45.4	44.1	43.1	40.0/35.4	43.6	0.5
0.2	43.1/42.6	50.6	37.9	38.8/47.7	43.9	6.4
0.4	38.1/39.4	22.9	39.1	33.9/40.2	33.4	9.1
0.5	40.1/41.1	53.4	38.2	37.8/44.0	43.9	8.3
0.6	43.8/41.9	40.9	45.6	42.3/47.7	43.4	2.4
0.7	40.9/39.9	32.6	39.3	62.6/42.3	37.6	4.4
0.8	41.0/43.7	36.6	41.1	48.6/33.2	39.6	2.6
1.0	39.9/42.3	31.0	43.6	59.8/46.1	38.2	6.5

The spectra were fit according to the above equations. All spectra were fit simultaneously for each sample. The data were fit using a personalized Mathcad routine for performing simultaneous nonlinear least-squares regressions. All peaks were fit to Lorentzian line shapes. It was assumed that all peaks associated with the methyl group and the methylene groups had the same widths, respectively. Observation of a relatively weak nonresonant background signal originating from the CaF_2 substrate warranted the introduction of a complex nonresonant background to each spectrum. While this contribution was generally on the order of 1−3% of the resonant signal intensities, inclusion of this contribution into the fitting procedure resulted in substantial improvements in the fits of the CH_3 asymmetric stretch region.

It is clear from Figure 7 that the fitting procedure is able to reproduce the experimentally observed spectra with good accuracy. The parameters used for the fits displayed in Figure 7 are presented in Table 2. The solid lines represent the best fits to the data. The most striking feature of these spectra is that the spectra of like polarization shown in Figure 7 appear considerably different as the composition is changed from 40% SN to 80% SN content. A close examination of the spectra indicates that the changes between these spectra are due primarily to modes associated with methylene group(s) and that there appears to be little change in the parameters associated with the terminal methyl group. Specifically, the most pronounced differences in the spectra are in the intensity of the methylene symmetric stretch at 2850 cm^{-1} and the methylene asymmetric and Fermi resonance bands in the 2900−2940 cm^{-1} spectral region. These differences are most notable in the PPP and SSP polarization combinations.

Various methods can and have been used to extract orientation information from SFG spectra.[16−25] To compare these methods we have employed four different approaches to determine orientation information. The first makes use of the intensities of the methyl symmetric stretch and the value of *R*. Unfortunately, the value of *R* is not well-known. Previous studies have used values ranging from 1.67 to 4.[16,19,22,23] Typically, the ratio of intensities of the symmetric stretch in the SPS and SSP polarization combinations is used to obtain the orientation. However, the SPS intensity is only a few percent of that of the SSP and is not often readily measurable with great accuracy. A second method relies on the ratio of symmetric stretch intensities in the SSP and PPP polarization combinations. While this SSP/PPP ratio is easily measurable, this method is subject to two difficulties, one being, extracting χ_{ZZZ} from the PPP spectrum, due to the large number of susceptibility elements that contribute to the signal in this polarization configuration, and the other being the extreme sensitivity of the Fresnel factor associated with the PPP polarization combination on the assumed refractive index of the film (*n*).[16,21] In the total internal reflectance geometry employed here, the Fresnel factor associated with χ_{ZZZ} is significantly larger than all others. On this basis, we assume that it is the only contributing factor for this polarization combination, significantly simplifying the situation. With an appropriate choice of *R* and *n*, the orientation can thus be deduced.

A third method makes use of the asymmetric stretch intensities. It has the advantage of being independent of the choice of *R*. The asymmetric stretch intensity ratio between the SPS and SSP polarization combinations could be used; however, in the SSP polarization combination, the asymmetric stretch mode interferes destructively with the Fermi resonance band, resulting in an asymmetric stretch feature that appears as a weak shoulder in the spectrum. In contrast, the interference between the asymmetric stretch and the Fermi resonance band in the PPP spectrum is constructive, and so the asymmetric stretch signal appears with considerable intensity, leading to a more reliable intensity determination and hence a more reliable orientation determination.

Finally, the ratio of intensities observed for the symmetric and asymmetric stretches can be used to determine the orientation if the ratio of $\alpha_{zxx}/\alpha_{zzz}$ is known. However, the value of this ratio is also not well-known and has been reported to range from 1 to 16.[19,22,23] This method is also restricted to the PPP polarization combination since it is the only polarization combination with significant intensity in both the symmetric and the asymmetric modes. While the parameters *R*, *n*′, and α_{zxx} used in these methods are subject to considerable uncertainty, one reasonable way of minimizing this is to fit the methyl intensities simultaneously for the various polarization combinations and try to find a single parameter set that yields a consistent set of orientation angles.

Through the use of the values $R = 2.4$, $n = 1.18$, and $\alpha_{zxx} = 4\alpha_{zzz}$, the orientation angle was calculated using the methods described above (method I, ratio of r− peak in SPS/PPP spectra (alternatively in the PSS/PPP spectra); method II, ratio of r+ peak in the SSP/PPP spectra; method III, ratio of r−/r+ in the PPP spectrum; method IV, ratio of r+ in SPS/SSP spectra (alternatively in the PSS/SSP spectra)). Table 2 shows the results of using the various methods to determine orientation information for mixed films ranging in composition from pure ferric stearate to pure stearonitrile. The table shows that, with a few notable exceptions, all methods give results in reasonable agreement with each other. It is interesting to note that for several different compositions method II appears to provide orientation angles with the greatest variability and at the extreme limits of the standard deviation. Nevertheless, our results indicate reasonable consistency in the methyl group orientation angles for all film compositions examined. The consistency of these angles is an indication of an appropriate choice for the

parameters set of R, α_{zxx}, and n. Method IV, with its small r+ SPS signal, on average, yielded consistently the same results.

For film compositions between 0% and 60% SN, the spectra in the CH region are characteristic of well-ordered, fully extended all-trans alkyl chains. Little intensity is observed in the methylene modes, consistent with a locally centrosymmetric environment in which oscillator strength from individual CH_2 groups of the alkyl chain is compensated for by adjacent groups. The averaged methyl group orientation angle obtained is ~44°, corresponding to a tilt angle of the alkyl chain of ~8° with respect to the surface normal assuming a rigid chain. At compositions of 70% SN and greater, there is a slight drop in the methyl group tilt angle by ~5°; however, this is still within the standard deviation of the values obtained for compositions <70% SN. However, upon examination of the corresponding spectra, it is clear that at compositions of >70% SN, there is a marked change in the intensities of the vibrational modes corresponding to the CH_2 group(s). The appearance of intensity in methylene modes can be attributed to either an increase in the number of gauche defects within the film, as has been observed in studies examining spectral signatures with increasing temperature, or to the possibility of other sources of uncompensated CH_2 oscillator strength within the alkyl chain such as localized chain bending or extended chain curvature.

In an attempt to discern between these possibilities, we have conducted atomic force microscopy studies on multilayer films of stearonitrile. It is reasonable to expect that if the observed intensity increases were due to an increase in the number of gauche defects, then, given the degree of CH_2 intensity in the spectra with a composition of 70% SN and greater, they would represent a significant number. We have observed clear signs of chain crystallization in molecular resolution AFM images of multilayer SN films. We argue that if the increase in intensity in the methylene modes were due to a substantial increase in the number of gauche defects within the film, then we would be unable to detect this level of chain crystallization. Rather, it is more likely that the increase in intensity of the CH_2 modes in films with a composition of 70% SN and greater results from either localized chain bending or extended chain curvature.

To examine whether this possibility could account for the observed spectral features, we have attempted to simulate the spectra associated with high SN compositions. This requires an analysis similar to that carried out previously for the methyl group vibrational modes, except that we must now relate the macroscopic susceptibility components to the microscopic hyperpolarizability components for the individual CH_2 modes.[26,27] The CH_2 unit has C_{2v} symmetry, and its nonvanishing hyperpolarizability tensor elements are α_{xxz}, α_{yyz}, and α_{zzz} for the symmetric stretch and $\alpha_{xzx} = \alpha_{zxx}$ for the asymmetric mode. For the CH_2 symmetric stretch mode (d+)

$$\chi_{yyz} = \chi_{xxz} = {}^1/_4 N[(\alpha_{xxz} + \alpha_{yyz} + 2\alpha_{zzz})\langle\cos\theta\rangle \times ((\alpha_{xxz} + \alpha_{yyz} - 2\alpha_{zzz})\langle\cos^3\theta\rangle)] \quad (12a)$$

$$\chi_{zzz} = {}^1/_2 N[(\alpha_{xxz} + \alpha_{yyz})\langle\cos\theta\rangle - ((\alpha_{xxz} + \alpha_{yyz} - 2\alpha_{zzz})\langle\cos^3\theta\rangle)] \quad (12b)$$

$$\chi_{yzy} = \chi_{zyy} = \chi_{xzx} = \chi_{zxx} = -{}^1/_4 N(\alpha_{xxz} + \alpha_{yyz} - 2\alpha_{zzz})[\langle\cos^3\theta\rangle] \quad (12c)$$

For the CH_2 asymmetric stretch mode (d−)

$$\chi_{yyz} = \chi_{xxz} = -{}^1/_2 N\alpha_{xzx}[\langle\cos\theta\rangle - \langle\cos^3\theta\rangle] \quad (13a)$$

$$\chi_{zzz} = \chi_{yyz} = N\alpha_{xzx}[\langle\cos\theta\rangle - \langle\cos^3\theta\rangle] \quad (13b)$$

$$\chi_{yzy} = \chi_{zyy} = \chi_{xzx} = \chi_{zxx} = {}^1/_2 N\alpha_{xzx}[\langle\cos^3\theta\rangle] \quad (13c)$$

These can be greatly simplified by known relationships between the nonvanishing elements of α,[26] namely, $\alpha_{xxz} + \alpha_{yyz} = 2\alpha_{zzz} \approx 0.98a_o$ and $\alpha_{xzx} \approx 0.66a_o$, where a_o is the polarizability constant of a single C−H bond. In our analysis the CH_2 Fermi resonance band was arbitrarily assumed to interact with the d+ mode to the same degree as the CH_3 Fermi resonance band does with the r+ mode.

Using the relationships between the susceptibility and hyperpolarizability components, we can simulate a spectrum based upon effective CH_2 and CH_3 tilt angles and oscillator strengths. This simple model is a great oversimplification, in that we assume there is only one source and magnitude of CH_2 oscillator strength. This model does not take into account any possible distributed nature of the CH_2 strength or position in the chain. Also, it does not take into account any spectral shifts or vibrational mode couplings that may be expected as a result of the introduction of significant bends or curvatures in the alkyl chains. Nevertheless, as the SFG spectra of stearonitrile in Figure 8 indicate, we can qualitatively reproduce the spectral features observed in the CH_2 region for pure SN films and for mixed films with a composition of >70% SN with this very simple model. These spectra are simulated assuming an oversimplified model in which the CH_2 contributions responsible for the intensity have an effective tilt angle of 50° and strength comparable to that of one methyl group. Unlike the curves of Figure 7, we are not attempting to fit our experimentally determined SFG spectra but rather predicting how the spectral features would change with different orientations of a methylene unit while keeping the methyl group angle fixed. We have applied a simplistic model and adjusted only the tilt angle of an effective methylene unit. Nevertheless, using only this single parameter we are able to reproduce *qualitatively* the characteristic spectral features that we see in all three polarization combinations of our SFG spectra for pure SN and their mixed films. Taking the spectra of pure stearonitrile as an example, we have set the methyl group to a tilt angle of 44° and adjusted the methylene tilt angle to 50°. This simple model predicts a large intensity for the CH_2 symmetric band in the PPP, a modest intensity in the SSP, and virtually no intensity in the SPS polarization combinations, respectively. The model also shows that the CH_2 asymmetric band has a rather large intensity in the PPP, virtually no intensity in the SSP, and a small intensity in the SPS polarization combinations, respectively. The model is also able to reasonably reproduce the relative intensities of the methylene bands in each polarization combination as well as the relative intensities of the methylene to the methyl peaks in all three polarization combinations.

It should be noted that when the methylene tilt angle is set to a value of 80° (that expected for a chain axis tilted from the surface normal by 10°) we are able to reproduce the spectra of films with a composition of <60% SN. In this context, we attribute the observed methylene intensity to either localized or extended deformations of the alkyl chains.

One potential explanation for the observed chain orientations is related to the electrostatic interactions between the headgroups of the stearonitrile amphiphiles. The CN headgroup is expected to possess a dipole moment on the order of 3.2 D.[1] A parallel alignment of dipoles of this magnitude at small separations is energetically unfavorable. The resulting repulsive interactions can be mitigated by an increase in the center-to-center angle

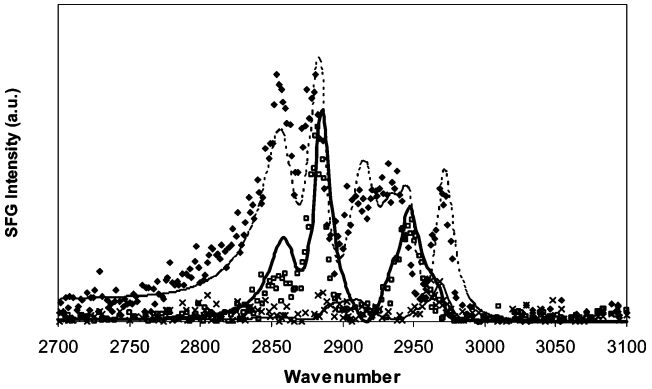

Figure 8. Diamonds, open squares, and X's represent the experimentally determined PPP, SSP, and SPS spectra of stearonitrile, respectively. Also shown are the calculated fits assuming Lorentzian line shapes with amplitudes corresponding to a methyl group tilt of 44° and an effective methylene group tilt of 50° (see text): PPP (dashed line), SSP (thick line), and SPS (thin line).

between the dipoles (i.e., a tilt). Such a response could result in an overall alkyl chain tilt or in a localized or somewhat extended bending of the alkyl chain. Given that our spectral fits indicate little to no difference in the averaged methyl group tilt angle with composition, we argue that such a scenario likely involves methylene units in proximity to the polar headgroup. Note that another method for mitigation of the repulsive interactions between CN headgroups is film dilution. It is possible that the introduction of ferric stearate relieves the dipole repulsion between headgroups to the extent that films with a composition of 70% SN or less undergo sufficient dilution to have their headgroups substantially less tilted and chains free of significant deformation. It is worth noting that the spectral differences appear to be correlated with differences in the $\pi-A$ isotherms and in the multilayer film deposition behavior. Even though the mono- and multilayer films studied here were deposited at surface pressures lower than that associated with the liquid condensed phase, it appears that the chain orientations of the amphiphiles are significantly different at higher SN compositions and play a key role in dictating the macroscopic properties of these films.

Conclusions

We have presented evidence for the control of multilayer film architecture through film composition. The spectral features of the monolayers corresponding to Z- and Y-type film deposition are distinct and characteristic for these structures. Monolayer films corresponding to polar, Z-type deposition display vibrational spectra with considerable intensity associated with methylene modes. This behavior is attributed to the presence of significant bends in the alkyl chains, likely in the proximity to the chain's polar headgroup. These chain deformations may result from large tilt angles associated with the polar CN headgroup, adopted to relieve dipole repulsive interactions. We are currently carrying out SFG experiments in the CN spectral region to probe the stearonitrile headgroup.

Attempts to provide more insight into the factors responsible for the spectral features observed here will require further SFG studies on isotopically substituted stearonitrile and diluants. Likewise, we are performing further AFM studies on multilayer films of varying composition to ascertain information regarding the amphiphilic chain structure and its correlation to macroscopic film properties.

Acknowledgment. The authors thank the Natural Sciences and Engineering Research Council of Canada and Simon Fraser University for financial support.

References and Notes

(1) Petty, M. C. *Langmuir Blodgett Films*; Cambridge University Press: New York, 1996.
(2) *Langmuir Blodgett Films*; Roberts, G., Ed.; Plenum Press: New York, 1990.
(3) *An Introduction to Ultrathin Organic Films*; Ulman, A., Ed.; Academic Press: New York, 1991.
(4) Popovitz-Biro, R.; Hill, K.; Shavit, E.; Hung, D. J.; Lahav, M.; Leiserowitz, L.; Sagiv, J.; Hsiung, H.; Meredith, G. R.; Vanherzeele, H. *J. Am. Chem. Soc.* **1990**, *112*, 2498.
(5) Popovitz-Biro, R.; Hill, K.; Landau, E. M.; Lahav, M.; Leiserowitz, L.; Sagiv, J.; Hsiung, H.; Meredith, G. R.; Vanherzeele, H. *J. Am. Chem. Soc.* **1988**, *110*, 2672.
(6) Serfis, A. B.; Katzenberger, R. *J. Colloid Interface Sci.* **1999**, *220*, 1.
(7) Cheong, D. W.; Kim, W. H.; Samuelson, L. A.; Kumar, J.; Tripathy, S. K. *Macromolecules* **1996**, *29* 1416.
(8) Teerenstra, M. N.; Hagting, J. G.; Schouten, A. J.; Nolte, R. J. M.; Kauranen, M.; Verbiest, T.; Persoons, A. *Macromolecules* **1996**, *29* 4876.
(9) Star, D.; Kikteva, T.; Leach, G. W. *J. Chem. Phys.* **1999**, *111*, 14.
(10) Copeland, L. E.; Harkins, W. D. *J. Am. Chem. Soc.* **1942**, *64*, 1600.
(11) Datta, A.; Sanyal, M. K.; Dhanabalan, A.; Major, S. S. *J. Phys. Chem. B.* **1997**, *101*, 9280.
(12) Davies, J. T.; Rideal, E. K. *Interfacial Phenomena*; Academic Press: New York, 1963.
(13) Romao, R. I. S.; Goncalves da Silva, A. M. *Chem. Phys. Lipids* **2004**, *131*, 27.
(14) MacPhail, R. A.; Strauss, H. L.; Snyder, R. G.; Elliger, C. A. *J. Phys. Chem.* **1984**, *88*, 334.
(15) Snyder, R. G.; Strauss, H. L.; Elliger, C. A. *J. Phys. Chem.* **1984**, *86*, 5145.
(16) Zhuang, X.; Miranda, P. B.; Kim, D.; Shen, Y. R. *Phys. Rev. B* **1999**, *59*, 19.
(17) Hirose, C.; Akamatsu, N.; Domen, K. *Appl. Spectrosc.* **1992**, *46*, 1051.
(18) Felderhof, B. U.; Bratx, A.; Marowsky, G.; Roders, O.; Sieverdes, F. *J. Opt. Soc. Am. B.* **1993**, *10*, 1924.
(19) Löbau, J.; Wolfrum, K. *J. Opt. Soc. Am. B* **1997**, *14*, 2505.
(20) Bell, R. B.; Bain, C. D.; Ward, R. N. *J. Chem. Soc., Faraday Trans.* **1996**, *92*, 515.
(21) Iimori, T.; Iwahashi, T.; Ishii, H.; Seki, K.; Ouchi, Y.; Ozawa, R.; Hamaguchi, H.; Kim, D. *Chem. Phys. Lett.* **2004**, *389*, 321.
(22) Harp, G. P.; Rangwalla, H.; Yeganeh, M. S.; Dhinojwala, A. *J. Am. Chem. Soc.* **2003**, *125*, 11283.
(23) Noguchi, H.; Ito, M.; Uosaki, K. *Chem. Lett.* **2005**, *34*, 950.
(24) Wolfrum, K.; Laubereau, A. *Chem. Phys. Lett.* **1994**, *228*, 83.
(25) Williams, C. T.; Yang, Y.; Bain, C. D. *Langmuir* **2000**, *16*, 2343.
(26) Lu, R.; Gan, W.; Wu, B.; Chen, H.; Wang, H. *J. Phys. Chem. B* **2004**, *108*, 7297.
(27) Lu, R.; Gan, W.; Wu, B.; Zhang, Z.; Guo, Y.; Wang, H. *J. Phys. Chem. B.* **2005**, *109*, 14118.